Nuclear shell evolution and in-medium NN interaction

N. A. Smirnova,[1] K. Heyde,[2] B. Bally,[1] F. Nowacki,[3] and K. Sieja[3]
[1]*CENBG (CNRS/IN2P3-Université Bordeaux 1) Chemin du Solarium, BP 120, 33175 Gradignan, France*
[2]*Department of Physics and Astronomy, Ghent University, Proeftuinstraat 86, B-9000 Ghent, Belgium*
[3]*Université de Strasbourg, IPHC, 23 rue du Loess 67037 Strasbourg France CNRS, UMR7178, 67037 Strasbourg, France*
(Received 22 July 2012; published 10 September 2012)

We report on a quantitative study of the evolution of the nuclear shell structure, in particular, effective single-particle energies (ESPEs), based on the spin-tensor decomposition of an effective two-body shell-model interaction. While the global trend of the ESPEs is mainly due to the central term of the effective interaction, variations of shell gaps invoke various components of the in-medium NN force. From a detailed analysis of a well-fitted realistic interaction in the $sdpf$ shell-model space, two most important contributions for the evolution of the $N=20$ and $N=28$ shell gaps are confirmed to be the central term and the tensor term. The role of the latter is dominant to explain the energy shift of spin-orbit partners. Spin-tensor analysis of microscopic effective interactions in sd, pf, and gds shell-model spaces, contrasted with that of the phenomenologically adjusted ones, shows no evidence of amplification of the tensor component contribution; however, it points toward the neglect of three-body forces in the present microscopic interactions.

DOI: 10.1103/PhysRevC.86.034314 PACS number(s): 21.10.Pc, 21.10.Jx, 21.30.Fe, 21.60.Cs

I. INTRODUCTION

The last few years have noticed a strongly increased activity, encompassing advanced experimental studies exploring energy spectra and electromagnetic properties [$B(E2)$ values, nuclear moments,...] and theoretical exploration of the nuclear shell model, in nuclei with a large neutron excess, even approaching the neutron drip line [1–3]. It has turned out that for nuclei with neutron number $N = 20$, 28, 40 (and their immediate vicinity) and with changing proton number, nuclear structure properties are observed that do not fit with a well closed neutron shell (for recent reviews see Refs. [2–7] and Refs. [1,8–12] and references therein). In particular, an onset of deformation and the presence of multiparticle multihole (mp-nh) intruder components in the ground states for neutron-rich nuclei around ^{32}Mg, ^{42}Si, and ^{64}Cr is well confirmed nowadays, both experimentally and theoretically (see, e.g., Refs. [1,13] and references therein). These are the regions of the nuclear chart called "islands of inversion." It turns out that for particular Z, N values, the correlation energy in these intruder configurations (quadrupole and pairing energy gain, mainly) is larger than the energy cost (because of the presence of large gaps in the single-particle energy spectrum) to create these intruder configurations. Consequently, the ground-state in both even-even (0^+) and in the odd-mass (J^π) nuclei becomes a strongly correlated state and subsequently gains extra binding. These islands of inversion do not imply inversions in the single-particle energies but rather a change in the ground-state configuration from a largely closed $N = 20$, 28, 40,... configuration into a strongly correlated one, including mp-nh excitations [1,14]. It immediately becomes clear that this energy balance will depend largely on the shell gaps and their variation as a function of proton number will play a major role. There are clear indications on single-particle energy variations in odd-A isotopes or isotones adjacent to semimagic nuclei, governed by the monopole term of the effective interaction (the so-called monopole shifts). Thus, it is but normal that the "standard" ordering of orbitals in a given major oscillator shell will change even causing new neutron N (or proton Z) numbers to give rise to an increased stability versus deformation, such as $N=14$ and $N=16$ in the O isotopes. A good description and understanding in order to predict the changing shell structure for the neutron-rich nuclei is highly important in the context of nuclear astrophysics.

The purpose of the present study is to investigate the changing shell structure using the nuclear shell-model framework and to understand the mechanisms behind these single-particle energies variations. This issue has been of central importance, as can be seen from the recent literature [15–21]. In particular, it has been shown that the spin-isospin exchange central and the tensor force components in the effective nuclear interaction play a major role in describing variations in the single-particle energy of a major shell [16,17,20,21]. Making use of a spin-tensor decomposition of the effective interaction [into its central, vector (symmetric and antisymmetric spin-orbit terms), and tensor rank-2 components], we show that global variation of the single-particle energy over a region of isotones (isotopes) is mainly due to the central part of the nucleon-nucleon interaction. On the other hand, the local variations (differences of single particle energies) in shell-gaps and in spin-orbit energy splitting are determined by the interplay of the central, vector, and tensor parts. We also study the differences in the spin-tensor decomposition between microscopic effective interactions (in-medium interactions starting from a realistic NN two-body force, where either a G matrix is constructed or a renormalized low-momentum force is constructed with the further addition of in-medium many-body effects using perturbation theory) and phenomenological effective interactions (the latter determined from fitting two-body matrix elements—or certain linear combinations of these matrix elements—to the wealth of experimental data). Comparison of the results obtained from using microscopic effective interactions and further adjusted to experimental data with phenomenological effective interactions allows us to formulate conclusions about the robustness of the proposed

mechanisms. In particular, there is no evidence for an enhancement of the tensor component in the renormalization process. Other components of the effective shell-model interaction do change in order to compensate for the neglect of the three-body forces.

We should mention at this place that the microscopic effective interactions, derived from the bare two-nucleon force (Bonn, Argonne, or chiral potentials) via a given renormalization procedure [22–24] have a problem since they do not give rise to the correct saturation and shell gaps observed in nuclei, which points to a defect in the monopole part of these interactions. Recent studies incorporating three-body terms in the effective force [25–27] have shown promising results, in particular, regarding extrapolations to new regions in the nuclear mass table where very few, or even no data exist. In many cases, an adjustment of the monopole term has been imposed to comply with the observed nuclear binding energies and spectroscopic evidence.

II. SHELL MODEL AND SPHERICAL MEAN-FIELD

Within the shell model, the spherical nuclear mean field is given by the monopole part [28–30] of the Hamiltonian, which contains only terms involving proton and neutron number operators (if the model space includes one or two neighboring major oscillator shells). It can be written as:

$$\hat{H}_{\rm mon} = \sum_i \epsilon_{\nu_i}\hat{n}_{\nu_i} + \sum_i \epsilon_{\pi_i}\hat{n}_{\pi_i} + \sum_{ij} V_{ij}^{\nu\pi}\hat{n}_{\nu_i}\hat{n}_{\pi_j} + \sum_{i\leqslant j}\frac{\hat{n}_{\nu_i}(\hat{n}_{\nu_j}-\delta_{ij})}{1+\delta_{ij}}V_{ij}^{\nu\nu} + \sum_{i\leqslant j}\frac{\hat{n}_{\pi_i}(\hat{n}_{\pi_j}-\delta_{ij})}{1+\delta_{ij}}V_{ij}^{\pi\pi}, \quad (1)$$

where $\hat{n}_{\pi_i}$ and $\hat{n}_{\nu_i}$ are proton and neutron number operators, i (j) refers to a complete set of quantum numbers of a harmonic oscillator orbital, and $V_{jj'}^{\rho\rho'}$ are centroids of the two-body interaction [28–30],

$$V_{ij}^{\rho\rho'} = \frac{\sum_J \langle ij|V|ij\rangle_J (2J+1)}{\sum_J (2J+1)}, \quad (2)$$

where ρ, ρ' denote protons or neutrons and the total angular momentum of a two-body state J runs over all values allowed by the Pauli principle.

The nucleon separation energies, calculated starting from the monopole Hamiltonian, are called *effective single-particle energies* (ESPEs). For a series of isotopes or isotones, they represent linear functions of the number of valence nucleons with respect to a reference nucleus (A_0):

$$\tilde{\varepsilon}_j^{\rho}(A) = \varepsilon_j^{\rho}(A_0) + \sum_{j'} V_{jj'}^{\rho\rho'}\langle\hat{n}_j^{\rho'}\rangle, \quad (3)$$

where j' runs over all valence orbitals.

These are the quantities to be compared with experimental single-particle centroids reconstructed from stripping and pick-up reactions [31]. In view of a recent paper on the concept of ESPEs [32], we stress that the present shell-model framework, as an approximation to the more general interacting many-body problem to describe atomic nuclei, provides us with a spherical mean-field as a consistent zeroth-order approximation. Detailed comparisons should, however, concentrate on comparing observable quantities such as one- and two-nucleon separation energies.

The higher-multipole part of the Hamiltonian, $\hat{H}_{\rm mult} = \hat{H} - \hat{H}_{\rm mon}$, contains particle-particle correlations—pairing, quadrupole-quadrupole correlations, and so on (see Ref. [33] for details).

The monopole part of the Hamiltonian describes the *spherical nuclear mean field*, favoring normal filling of orbitals and defining magic numbers. Its single-particle states, or ESPEs, provide an important ingredient for the formation of shells and the interplay between spherical configurations and deformation in nuclei. The higher multipole part of the interaction provides the so-called *correlation energy* for particle-hole excitations across the shell gap. Large shell gaps are a prerequisite in order to obtain rigid magic numbers. A reduction of the spherical shell gaps may lead to the formation of a deformed ground state, if the correlation energy of a given excited (intruder) configuration is large enough to overcome the cost in energy in making the excited configuration [14].

III. SHELL EVOLUTION AND NUCLEAR FORCES

The question as to which term of the nuclear force is mainly responsible to describe the observed nuclear shell evolution has been the interest of nuclear structure studies for a long time [29,30,34]. In particular, in Ref. [15] from the analysis of the ESPEs in p and sd shell nuclei, it was noticed that the proton-neutron centroids involving spin-orbit partners are large and attractive and that this is a property inherent to the spin-isospin-exchange term of the central force, $V = f(r)(\vec{\sigma}_1 \cdot \vec{\sigma}_2)(\vec{\tau}_1 \cdot \vec{\tau}_2)$.

It was recognized, however, when analyzing the behavior of ESPEs throughout the nuclear chart [16] that proton-neutron centroids of the type $V^{\pi\nu}_{nlj_>,n'l'j'_<}$ or $V^{\pi\nu}_{nlj_<,n'l'j'_>}$ ($j_{\gtrless}$ denote aligned and opposite spin-orbital orientation partner for a given l) were systematically large and attractive even though, in general, $l \neq l'$. This required a noncentral force and was in agreement with the characteristic property of a tensor operator $V = f(r)[\vec{\sigma}_1 \times \vec{\sigma}_2]^{(2)} \cdot Y^{(2)}(\vec{\tau}_1 \cdot \vec{\tau}_2)$, namely $(2j_> + 1)V^{\pi\nu}_{j_>j'} + (2j_< + 1)V^{\pi\nu}_{j_<j'} = 0$ [16]. Thus, it was suggested that it was a tensor force that governed the shell structure in a major way. The authors of Ref. [16] have evaluated experimental shifts of single-particle energies in Ca-isotopes, $N = 51$ isotones, and Sb-isotopes using a schematic tensor force.

Since then, numerous efforts have been carried out with the aim to incorporate a tensor force in a consistent way within the mean-field models (Refs. [10,35–37] and references therein). Until recently, most of the mean-field calculations based on Skyrme or Gogny density functional parametrizations had not considered a tensor term.

There is still a need for a better understanding of the contribution originating from the tensor force in the effective nucleon-nucleon interaction and there is a demand for its firm signatures. A quantitative approach to determine the role of different terms of the effective shell-model interaction in

the evolution of the shell gaps is provided by studying their spin-tensor decomposition.

Another crucial aspect of shell evolution concerns the role of the three-nucleon forces. For a long time, it was not understood why NN realistic interactions failed to reproduce spin-orbit shell closures, like those in ^{48}Ca and ^{56}Ni. The evolution of such gaps is one of the central problems of nuclear structure: when the orbital with the largest angular momentum in a major shell fills, it binds itself and contributes to the binding of the orbitals with the largest angular momentum in neighboring shells in a way that NN forces fail to reproduce. It is this orbital with the largest angular momentum in the oscillator shell N that drops in energy and becomes an unnatural parity orbital in the $N-1$ oscillator shell. As a consequence, it follows that the pure two-body forces are unable to produce the spin-orbit shell closures at $N, Z =$ 14, 28, 50, 82, and 126. A deeper insight into this problem came from recognizing the importance to modify the monopole field, resulting in changes of energy centroids, as emphasized by Poves and Zuker [29], and later, when the connection with missing $3N$ monopole forces in nuclear structure calculations was suggested [25]. It was also shown (see Ref. [25]) that major problems encountered in describing nuclear energy spectra using shell-model calculations with NN interactions in the p, sd, and pf shells could be remedied by adding three-nucleon forces. The proposed $3N$ mechanism has been further validated in light systems by no-core shell-model calculations, including three-nucleon forces [38]. Since the phenomenological monopole corrections are indeed due to the missing three-body contributions, the spin-tensor decomposition of empirically adjusted interactions on one hand and of the realistic in-medium interactions on the other, can provide a quantitative insight into the role and the spin-isospin structure of $3N$ components contributing to the creation of spin-orbit closures.

IV. SPIN-TENSOR DECOMPOSITION OF THE TWO-BODY INTERACTION

Any two-nucleon interaction can be expanded using a decomposition as a sum of a scalar, vector and rank-2 spherical tensor,

$$V = \sum_{k=0,1,2} [S^{(k)} \cdot Q^{(k)}] = \sum_{k=0,1,2} V^{(k)}, \tag{4}$$

where $S^{(k)}$ are spin-tensors constructed from nucleon spin-1/2 operators and $Q^{(k)}$ are corresponding rank tensors in the coordinate space. For the spin part, one can construct scalar operators [1 and $(\vec{\sigma}_1 \cdot \vec{\sigma}_2)$] contributing to the central part of the effective interaction, the rank-2 term $[(\vec{\sigma}_1 \times \vec{\sigma}_2)^{(2)}]$ describing the so-called tensor force, while the vector part $(k=1)$ includes a term $\vec{\sigma}_1 + \vec{\sigma}_2$, contributing to the usual two-body spin-orbit force and two more operators that exchange the intrinsic spin in LS-coupled basis and are called the *antisymmetric spin-orbit* (ALS) operators $[(\vec{\sigma}_1 \times \vec{\sigma}_2)^{(1)}$ and $\vec{\sigma}_1 - \vec{\sigma}_2]$. Using the LS scheme, it is possible to calculate the matrix elements of each $V^{(k)}$ component of the interaction from the matrix elements of V:

$$\begin{aligned}\langle (nl, n'l' : LS, JMTM_T | V^{(k)} | n''l'', n'''l''' : L'S', JMTM_T \rangle \\ = (2k+1)(-1)^J \begin{Bmatrix} L & S & J \\ S' & L' & k \end{Bmatrix} \sum_{J'} (-1)^{J'} (2J'+1) \begin{Bmatrix} L & S & J' \\ S' & L' & k \end{Bmatrix} \\ \times \langle nl, n'l' : LS, J'MTM_T | V | n''l'', n'''l''' \\ \times : L'S', J'MTM_T \rangle. \end{aligned} \tag{5}$$

Based on the selection rules in LS coupling, it is even possible to discriminate between triplet-even (TE), triplet-odd (TO), singlet-even (SE), and single-odd (SO) terms of the central part, between even and odd components of the spin-orbit term (LS and ALS, respectively) and even and odd components of the tensor term (TNE and TNO, respectively). The specific contribution of these terms to the centroids of the interaction and, thus, to the ESPE variations is additive.

The spin-tensor decomposition was used to study the tensorial structure of effective interactions in a number of publications [18,19,39–44]. The analysis focused on the two-body matrix elements and/or centroids of the interaction, even in the context of the ESPE variations [19]. In particular, in Refs. [18,19], the dominant role of the central term was discovered, in contradiction with the results of Ref. [16].

Recently, we have analyzed the evolution of the spherical *shell gaps*, governed by the *differences* between two centroids, which elucidated an equal importance of both the central and the tensor term to describe the evolution of the ESPEs [21].To illustrate this, let us consider the evolution of the $N=20$ shell gap in the $N=20$ isotones between Ca and O. Figure 1(a) shows the corresponding neutron ESPEs, constructed starting from the realistic effective interaction adjusted to experimental data (SPDF-U) as described in Ref. [45]. The $N=20$ shell gap is given by the differences between the proton-neutron centroids of the two-body interaction, involving the neutron $0d_{3/2}$ and $0f_{7/2}$ orbitals. Here, we focus the discussion on two regions, when protons fill the $0d_{5/2}$ and $0d_{3/2}$ orbitals, respectively. Therefore, we compare the centroids $V^{\nu\pi}_{0f_{7/2}0d_{3/2}}$ versus $V^{\nu\pi}_{0d_{3/2}0d_{3/2}}$ and $V^{\nu\pi}_{0f_{7/2}0d_{5/2}}$ versus $V^{\nu\pi}_{0d_{3/2}0d_{5/2}}$. The results of the corresponding spin-tensor decomposition are shown in Table I. We notice that the contribution of the tensor force to the full centroids under consideration is below 20%. The main contribution is due to the central term of the force, in particular, in its triplet-even channel. However, in order to describe the shell gaps, we have to consider differences between the centroids, given in Table I as well (columns labeled as ΔV). Here, one notices that the tensor component becomes equally important to the central component. When protons are removed from the $0d_{3/2}$ orbital, there appears an almost exact compensation between the central and tensor contributions to the $N=20$ shell gap variation. Consequently, going from ^{40}Ca to ^{36}Si, this shell gap persists. However, when protons are removed from the $0d_{5/2}$ orbital (from ^{34}Si downwards to the unbound nucleus ^{28}O), the central and tensor contributions to the difference between the centroids have the same sign and this causes a drastic reduction of the $N=20$ shell gap, leading to development of the "island of inversion."

In the same way we have analyzed the evolution of the the $N=28$ shell gap in the $N=28$ isotones starting from ^{48}Ca

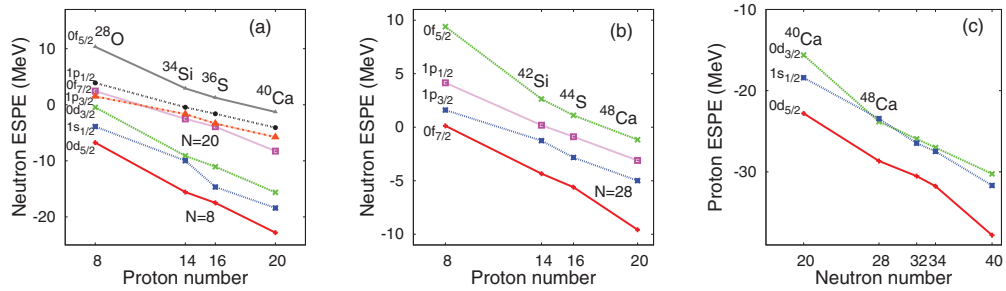

FIG. 1. (Color online) Neutron ESPEs in $N = 20$ isotones (a); in $N = 28$ isotones (b) and proton ESPEs in Ca isotopes (c), as obtained from the realistic interaction [45].

and approaching the lighter nuclei [Fig. 1(b)]. This shell gap results from the difference in the centroids corresponding to the neutron $1p_{3/2}$ and $0f_{7/2}$ orbitals, which are both "spin-up" ($j_> = l + 1/2$) orbitals but have different radial quantum numbers. Hence, the tensor force contributes to both centroids, $V^{\nu\pi}_{1p_{3/2}0d_{3/2}}$ and $V^{\nu\pi}_{0f_{7/2}0d_{3/2}}$ with equal sign, but the absolute values are quite different (see the lower part of Table II). As a result, the tensor contribution to the shell-gap variation is about half of that of the central contribution when the proton $0d_{3/2}$ orbital is filled and about $1/3$ of it, but with the opposite sign, when the proton $0d_{5/2}$ orbital is being filled. Thus, we observe a gradual reduction of the $N = 28$ shell gap moving from ^{48}Ca to ^{44}S and an even more rapid reduction of this shell gap from ^{42}Si toward even lighter isotones. In conclusion, we stress again that the behavior of a given ESPE is governed mainly by the triplet-even component of the central part. However, evolution of the shell gap is influenced by both central and tensor components of the effective interaction, not always having the same sign.

The only example when the effect of the central part is negligible is provided by the evolution of the spin-orbit splitting. This is illustrated by the analysis of the proton $0d_{3/2}$-$0d_{5/2}$ splitting between ^{40}Ca and ^{48}Ca (Fig. 1(c) and Ref. [21]), the decrease of -2.3 MeV is mainly due to the tensor contribution (-2.73 MeV) with only a small contribution stemming from the central term (-0.21 MeV) and a contribution from the vector term (0.6 MeV). Thus, the energy shift for spin-orbit partners in opposite senses, when they result from centroids [here the $(1f_{7/2})$-(2d) centroids] governed by cross-shell proton-neutron matrix elements, are indeed mainly due to the tensor force.

To specify, let us remark that calculations of the shell gap evolution from an effective interaction, as presented here, take into account a well-established mass dependence on the two-body matrix elements, expressed by a scaling factor $(A/A_0)^{-1/3}$ [46,47]. Therefore, to obtain the change of a given energy gap, it is not sufficient to multiply the differences in two-body centroids given in Tables I and II by a number of added particles, only.

In conclusion, while the global trend of the ESPEs is due mainly to the central term of the effective interaction, evolution of the shell gaps is a common effect, dominantly, of the central and tensor terms. The characteristic properties of the tensor force are manifested in the analysis of the spin-orbit splitting. From our analysis, the role of the vector term is small and it often contributes to the differences between centroids in the way opposite to the tensor force contribution.

V. MICROSCOPIC VERSUS PHENOMENOLOGICAL INTERACTION

The goal of the shell model is to describe nuclear structure properties starting from microscopic effective interactions. However, at present the effective interactions derived from a bare NN force by some renormalization procedure based on a G matrix or using a low-momentum interaction $V_{\mathrm{low}-k}$ plus higher-order corrections within the many-body perturbation

TABLE I. Spin-tensor content of the centroids of the realistic interaction SDPF-U [45] involved into the evolution of the $N = 20$ shell gap.

Centroid	$V^{\nu\pi}_{0f_{7/2}0d_{3/2}}$ MeV	$V^{\nu\pi}_{0d_{3/2}0d_{3/2}}$ MeV	ΔV MeV	$V^{\nu\pi}_{0f_{7/2}0d_{5/2}}$ MeV	$V^{\nu\pi}_{0d_{3/2}0d_{5/2}}$ MeV	ΔV MeV
Total	**−1.70**	**−1.79**	**0.09**	**−1.32**	**−2.04**	**0.72**
Central	**−1.51**	**−2.17**	**0.66**	**−1.48**	**−1.90**	**0.43**
TE	−1.35	−2.17	0.82	−1.46	−1.89	0.44
Vector	**0.09**	**0.06**	**0.03**	**−0.03**	**0.08**	**−0.11**
LS	0.00	0.07	0.07	−0.03	0.01	−0.04
ALS	0.09	−0.01	0.10	0.00	0.07	−0.07
Tensor	**−0.28**	**0.32**	**−0.60**	**0.19**	**−0.22**	**0.40**
even	−0.16	0.24	−0.40	0.11	−0.16	0.27
odd	−0.12	0.09	−0.20	0.08	−0.06	0.13

TABLE II. Spin-tensor content of the centroids of the realistic interaction SDPF-U [45] involved into the evolution of the $N = 28$ shell gap.

Centroid	$V^{\nu\pi}_{1p_{3/2}0d_{3/2}}$ MeV	$V^{\nu\pi}_{0f_{7/2}0d_{3/2}}$ MeV	ΔV MeV	$V^{\nu\pi}_{1p_{3/2}0d_{5/2}}$ MeV	$V^{\nu\pi}_{0f_{7/2}0d_{5/2}}$ MeV	ΔV MeV
Total	**−1.06**	**−1.70**	**0.64**	**−0.95**	**−1.32**	**0.36**
Central	**−1.04**	**−1.51**	**0.47**	**−1.03**	**−1.48**	**0.44**
TE	−0.99	−1.35	0.36	−1.02	−1.46	0.44
Vector	**0.05**	**0.09**	**−0.05**	**0.04**	**−0.03**	**0.07**
LS	0.06	0.00	0.06	0.00	−0.03	−0.03
ALS	−0.01	0.09	−0.10	0.04	0.00	0.04
Tensor	**−0.06**	**−0.28**	**0.22**	**0.04**	**0.19**	**−0.15**
even	−0.02	−0.16	0.14	0.02	0.11	−0.09
odd	−0.04	−0.12	0.08	0.02	0.08	−0.06

theory do not result in a correct description of the nuclear structure properties and fail to reproduce shell closures and single-particle behavior [24,29]. To improve the descriptive power, shell-model practitioners perform an empirical adjustment of such interactions either by correcting the monopole part to experimental data or by using a least-squares fit of all two-body matrix elements to the experimental nuclear structure data (see, e.g., Refs. [1,45,46,48,49]). It appears that in the latter the major changes concern also the monopole part.

In order to understand how the effective monopole interaction changes by such adjustments, we analyze the shell gaps in three consecutive model spaces, each comprising one major harmonic oscillator shell: $(1s0d)$, $(1p0f)$, and $(0g1d2s)$, using both microscopic and adjusted realistic effective interactions. In Figs. 2(a), 3(a), and 4(a), we show the neutron ESPEs in the O isotopes, Ca isotopes, and Zr isotopes, respectively, obtained from the microscopic effective interactions, based on the G matrices and including core-polarization and higher-order diagrams. The interaction for the sd shell-model space is taken from Ref. [22] (renormalized G matrix applied to the sd shell—RG-SD, which is based on the Bonn-A potential), while for the pf shell-model space we use the KB interaction from Ref. [50] and for the gds shell-model space we use a renormalized G matrix based on the CD-Bonn potential (RG-GDS) [22,51]. In Figs. 2(b), 3(b), and 4(b), we show

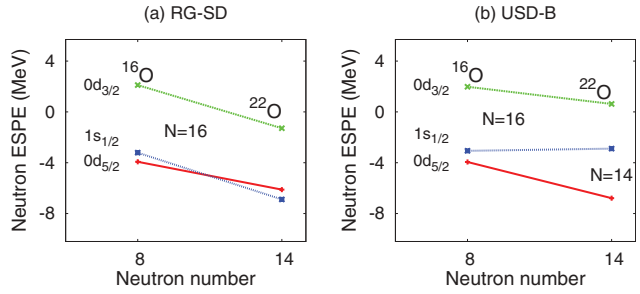

FIG. 2. (Color online) Neutron ESPEs in O isotopes calculated with the microscopic effective interaction (a) and the adjusted effective interaction (b).

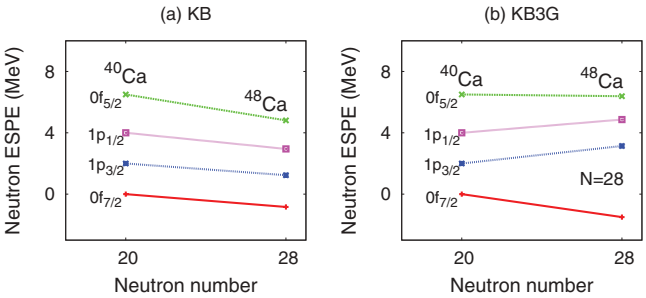

FIG. 3. (Color online) Neutron ESPEs in Ca isotopes calculated with the microscopic effective interaction (a) and the adjusted effective interaction (b).

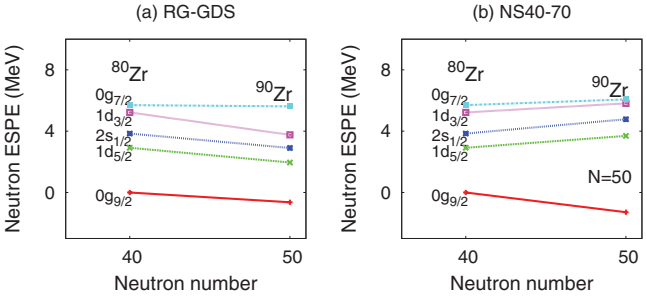

FIG. 4. (Color online) Neutron ESPEs in Zr isotopes calculated with the microscopic effective interaction (a) and the adjusted effective interaction (b).

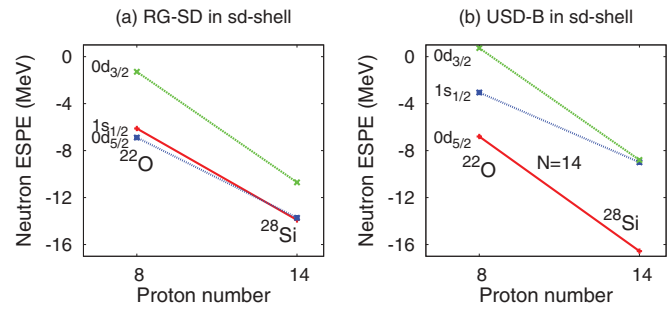

FIG. 5. (Color online) Neutron ESPEs in $N = 14$ isotones from ^{22}O to ^{28}Si calculated with the microscopic effective interaction (a) and the adjusted effective interaction (b).

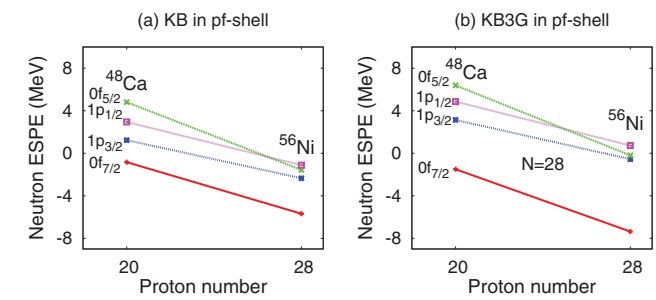

FIG. 6. (Color online) Neutron ESPEs in $N = 28$ isotones from ^{48}Ca to ^{56}Ni calculated with the microscopic effective interaction (a) and the adjusted effective interaction (b).

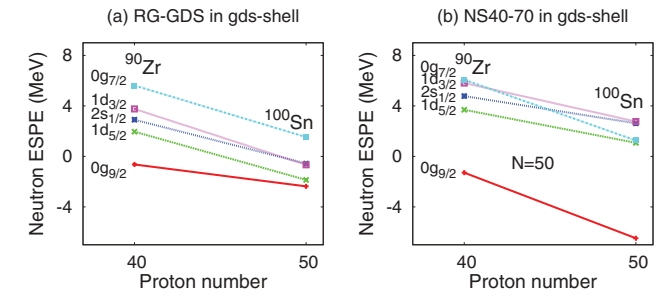

FIG. 7. (Color online) Neutron ESPEs in $N = 50$ isotones from ^{90}Zr to ^{100}Sn calculated with the microscopic effective interaction (a) and the adjusted effective interaction (b).

TABLE III. Spin-tensor decomposition of the $N=14$ shell-gap evolution and the $\nu(0d_{3/2}\text{-}0d_{5/2})$ spin-orbit splitting in the O isotopes (columns 2 and 3, 8 and 9), of the $N=28$ shell-gap evolution and the $\nu(0f_{5/2}\text{-}0f_{7/2})$ spin-orbit splitting in the Ca isotopes (columns 4 and 5, 10 and 11) and of the $N=50$ shell-gap evolution and the $\nu(0g_{7/2}\text{-}0g_{7/2})$ spin-orbit splitting in Zr isotopes (columns 6and 7, 12 and 13).

Energy gap	$\nu(0d_{5/2}\text{-}1s_{1/2})$ MeV		$\nu(0f_{7/2}\text{-}1p_{3/2})$ MeV		$\nu(0g_{9/2}\text{-}1d_{5/2})$ MeV		$\nu(0d_{5/2}\text{-}0d_{3/2})$ MeV		$\nu(0f_{7/2}\text{-}0f_{5/2})$ MeV		$\nu(0g_{9/2}\text{-}0g_{7/2})$ MeV	
Filling orbital	$\nu 0d_{5/2}$ $^{16}\text{O}\rightarrow{}^{22}\text{O}$		$\nu 0f_{7/2}$ $^{40}\text{Ca}\rightarrow{}^{48}\text{Ca}$		$\nu 0g_{9/2}$ $^{80}\text{Zr}\rightarrow{}^{90}\text{Zr}$		$\nu 0d_{5/2}$ $^{16}\text{O}\rightarrow{}^{22}\text{O}$		$\nu 0f_{7/2}$ $^{40}\text{Ca}\rightarrow{}^{48}\text{Ca}$		$\nu 0g_{9/2}$ $^{80}\text{Zr}\rightarrow{}^{90}\text{Zr}$	
	RG-SD	USD-B	KB	KB3G	RG-GDS	NS40-70	RG-SD	USD-B	KB	KB3G	RG-GDS	NS40-70
Total	**−1.48**	**3.01**	**0.07**	**2.73**	**−0.32**	**2.05**	**−1.21**	**1.49**	**−0.85**	**1.43**	**0.56**	**1.66**
Central	**−0.22**	**1.89**	**0.49**	**1.21**	**−0.06**	**0.07**	**−1.16**	**−0.51**	**−0.31**	**0.0**	**0.96**	**−0.38**
TO	−0.82	1.31	−0.24	0.23	−0.35	−0.45	−0.18	0.06	−0.10	−0.07	−0.26	−0.07
SE	0.60	0.56	0.73	0.98	0.29	0.52	−0.98	−0.57	−0.21	0.07	1.22	−0.31
Vector	**−0.77**	**1.26**	**0.04**	**1.64**	**0.04**	**1.70**	**1.16**	**2.29**	**0.83**	**2.01**	**0.59**	**1.85**
LS	−0.83	0.27	−0.03	0.52	−0.01	0.49	0.27	0.35	0.17	0.34	0.11	0.29
ALS	0.06	0.99	0.07	1.12	0.05	1.21	0.89	1.94	0.66	1.67	0.48	1.56
Tensor	**−0.49**	**−0.12**	**−0.46**	**−0.12**	**−0.30**	**0.28**	**−1.21**	**−0.29**	**−1.37**	**−0.58**	**−0.99**	**0.19**

the same ESPEs as in panels (a) but obtained from the phenomenologically adjusted USD-B interaction [49] for the O isotopes, from the KB3G interaction [52] for the Ca isotopes and from a monopole-adjusted interaction recently used in Refs. [53–55] named hereafter NS40-70 for Zr isotopes.

In Table III we present a detailed spin-tensor analysis of the $N=14$ shell gap evolution (splitting between the neutron $1s_{1/2}$ and $0d_{5/2}$ orbitals) for the O isotopes, of the $N=28$ shell gap evolution (splitting between the neutron $1p_{3/2}$ and $0f_{7/2}$ orbitals) for the Ca isotopes, and of the $N=50$ shell gap evolution (splitting between the neutron $0g_{9/2}$ and $1d_{5/2}$ orbitals) for the Zr isotopes.

Although the model spaces are different and the adjustments of the interactions were carried out in different ways, the results of the decomposition are remarkably similar. All the realistic interactions do not describe an increase of the $N=14$, $N=28$, and $N=50$ shell gaps when neutrons fill the $0d_{5/2}$, $0f_{7/2}$, and $0g_{9/2}$ orbitals, respectively. Phenomenological adjustment to the experimental data increases both gaps by an amount of 2–3 MeV. An extra repulsion of the $T=1$ monopoles is introduced partially in the central component, partially in the vector part (especially its ALS component) and by the reduction of the tensor attraction.

Qualitatively similar results can be obtained from the analysis of the spin-tensor decomposition of the spin-orbit splitting evolution [$\nu(0d_{3/2}\text{-}0d_{5/2})$ splitting in O isotopes and $\nu(0f_{5/2}\text{-}0f_{7/2})$ splitting in Ca isotopes; see Table III]. A slight difference with respect to O and Ca chains can be noted in Zr isotopes (columns 12–13 in Table III), where the central term contribution to the spin-orbit splitting becomes more attractive in the empirical adjustment of the interaction. One should note that, contrary to the *sd* and *pf* shells, the realistic interaction used in the *gds* shell does not lead to the reduction of the spin-orbit splitting between ^{80}Zr and ^{90}Zr. Otherwise, the vector contribution is enhanced and the tensor attraction reduced in the empirical monopole adjustment, in full analogy to lighter nuclei. In all the empirical interactions, the major contribution to the spin-orbit splittings is provided by the $T=1$ vector term.

Let us now discuss the role of different components in the proton-neutron part of the interaction. In Figs. 5(a) and 5(b), we present the evolution of the neutron ESPEs in the $N=14$ isotones when filling the proton $\pi 0d_{5/2}$ orbital (i.e., between ^{22}O and ^{28}Si) obtained with a realistic RG-SD interaction

TABLE IV. Spin-tensor decomposition of the $N=14$ shell-gap evolution in $N=14$ isotones (columns 2 and 3), $N=28$ shell-gap evolution in $N=28$ isotones (columns 4 and 5), and $N=50$ shell-gap evolution in $N=50$ isotones (columns 6 and 7) as well as of the $\nu(0d_{5/2}\text{-}0d_{3/2})$ spin-orbit splitting in $N=14$ isotones (columns 8 and 9), $\nu(0f_{5/2}\text{-}0f_{7/2})$ spin-orbit splitting in $N=28$ isotones (columns 10 and 11), and of the $\nu(0g_{9/2}\text{-}0g_{7/2})$ spin-orbit splitting in $N=50$ isotones (columns 12 and 13).

Energy gap	$\nu(0d_{5/2}\text{-}1s_{1/2})$ MeV		$\nu(0f_{7/2}\text{-}0p_{3/2})$ MeV		$\nu(0g_{9/2}\text{-}1d_{5/2})$ MeV		$\nu(0d_{5/2}\text{-}0d_{3/2})$ MeV		$\nu(0f_{7/2}\text{-}0f_{5/2})$ MeV		$\nu(0g_{9/2}\text{-}0g_{7/2})$ MeV	
Filling orbital	$\pi 0d_{5/2}$ $^{22}\text{O}\rightarrow{}^{28}\text{Si}$		$\pi 0f_{7/2}$ $^{48}\text{Ca}\rightarrow{}^{56}\text{Ni}$		$\pi 0g_{9/2}$ $^{90}\text{Zr}\rightarrow{}^{100}\text{Sn}$		$\pi 0d_{5/2}$ $^{22}\text{O}\rightarrow{}^{28}\text{Si}$		$\pi 0f_{7/2}$ $^{48}\text{Ca}\rightarrow{}^{56}\text{Ni}$		$\pi 0g_{9/2}$ $^{90}\text{Zr}\rightarrow{}^{100}\text{Sn}$	
	RG-SD	USD-B	KB	KB3G	RG-GDS	NS40-70	RG-SD	USD-B	KB	KB3G	RG-GDS	NS40-70
Total	**0.95**	**3.82**	**1.27**	**2.39**	**−2.08**	**2.58**	**−1.63**	**0.23**	**−1.53**	**−0.75**	**−2.35**	**0.39**
Central	**2.58**	**3.59**	**2.11**	**2.90**	**−1.24**	**1.67**	**0.26**	**0.45**	**0.23**	**0.47**	**−0.40**	**0.17**
TE	2.25	2.96	2.04	2.51	0.04	1.24	0.95	1.99	0.61	0.59	0.53	0.31
Vector	**−0.87**	**0.90**	**−0.09**	**0.33**	**−0.15**	**1.41**	**0.0**	**1.45**	**0.50**	**1.25**	**0.25**	**1.79**
LS	−0.72	0.41	−0.14	−0.07	−0.13	0.68	−0.24	0.72	0.08	0.34	0.01	0.76
ALS	−0.15	0.49	0.06	0.40	−0.02	0.72	0.24	0.73	0.42	0.91	0.24	1.03
Tensor	**−0.76**	**−0.68**	**−0.74**	**−0.84**	**−0.69**	**−0.50**	**−1.89**	**−1.67**	**−2.26**	**−2.47**	**−2.20**	**−1.57**

and with the adjusted USD-B interaction [49], respectively. The evolution of the ESPEs in the $N=28$ isotones, going from ^{48}Ca to ^{56}Ni, obtained from the KB and KB3G effective interactions is shown in Figs. 6(a) and 6(b). The analogous situation in the gds shell nuclei is displayed in Figs. 7(a) and 7(b), where the evolution of neutron ESPE in the $N=50$ isotones is plotted between ^{90}Zr and ^{100}Sn. We focus our analysis on the variations of the neutron $(0d_{5/2}$-$0d_{3/2})$ spin-orbit splitting in the sd shell, of the neutron $(0f_{5/2}$-$0f_{7/2})$ spin-orbit splitting in the pf shell, of the neutron $(0g_{9/2}$-$0g_{7/2})$ spin-orbit splitting in the gds shell, and of the neutron $(0d_{5/2}$-$1s_{1/2})$, $(1p_{3/2}$-$0f_{7/2})$, and $(1d_{5/2}$-$0g_{9/2})$ energy differences (the $N=14$, $N=28$, and $N=50$ shell gaps, respectively). The contributions from different components to these energy differences are summarized in Table IV.

As could be inferred already from Figs. 2–4, the realistic interactions (RG-SD, KB, RG-GDS) predict too small gaps and spin-orbit splittings in ^{22}O, ^{48}Ca, and ^{90}Zr, which results in the absence of magic properties of these nuclei. We will, however, for the moment, concentrate on the increase of both splittings moving from ^{22}O, ^{48}Ca, and ^{90}Zr onwards, when protons are added.

One notices that the RG-SD (KB) interaction predicts a larger reduction of the $\nu 0d_{5/2}$-$0d_{3/2}$ $[\nu(0f_{5/2}$-$0f_{7/2})]$ spin-orbit splitting going from ^{22}O to ^{28}Si (^{48}Ca to ^{56}Ni) than the USD-B (KB3G) interaction (see Figs. 5 and 6 and Table IV, columns 8–11). The decrease of this particular spin-orbit splitting, while protons are added in the $0d_{5/2}$ $(0f_{7/2})$ orbital, is a characteristic feature of the tensor force. It is remarkable that the contribution of the tensor components change very little and it is the vector term that changes drastically.

In heavier nuclei, between ^{90}Zr and ^{100}Sn, the largest contribution to the spin-orbit partners evolution is provided by the modification in the vector term, as in the lighter systems. The reduction of the tensor attraction appears, however, stronger than in the sd and pf cases.

Similar conclusions to those obtained from spin-orbit splittings analysis can be made from the analysis of the $N=14, 28, 50$ shell gaps. The realistic interactions do not result into a sufficient increase of this gap while going from ^{22}O to ^{28}Si, ^{48}Ca to ^{56}Ni, and ^{90}Zr to ^{100}Sn. The empirical interactions, on the other hand, result in an important increase, resulting from significant and additive contributions from the dominant central and vector terms (see Table IV, columns 2–7). As before, the contribution of the proton-neutron tensor component is of minor importance. It is crucial to note that empirical adjustments of the interaction almost do not alter the contribution of the tensor force and that the absolute magnitude of this contribution to a given shell gap evolution is fairly similar, irrespective of the mass region.

As a result, we are tempted to conclude from the examples discussed before that the adjustments made to modify the starting microscopically derived effective interaction into a phenomenological interaction do not produce any significant enhancement of the proton-neutron tensor effect. These results support the analysis of Ref. [56] on the renormalization persistence of the tensor force. Even more, we notice that adjustments of the microscopic interactions, in particular the ones that imply modifications of the monopole term to make it consistent with the experimental data, do not alter much the tensor component of the proton-neutron effective interaction. It appears that these are the central and vector components that exhibit major changes in modifying the interaction from realistic to empirically adjusted versions. Consequently, these are also the terms which are most sensitive to the neglect of the three-nucleon forces responsible for the occurrence of the spin-orbit shell closures.

VI. SUMMARY AND CONCLUSIONS

The spin-tensor decomposition of the two-body interaction is shown to provide a quantitative and unambiguous way to determine the role played by the different terms of the in-medium nuclear force in the study of the shell evolution in nuclei far from stability. It is shown that both the central and tensor terms play a crucial role in our understanding of the evolution of the shell gaps at $N=20$ and $N=28$ (in line with Ref. [20]), while the tensor term being dominant for the evolution of the spin-orbit splitting governed by cross-shell proton-neutron centroids (one of possible signatures).

We have also shown that an empirical adjustment of microscopic two-body effective interactions, due to missing three-nucleon interactions, introduces an overall repulsion in the $T=1$ monopoles and results mainly in enhancing the central and vector terms, as well as in reducing the tensor term contribution. Modifications of the tensor term contribution to the shell-gaps evolution by an adjustment of the $T=0$ tensor monopoles appear to be minor. A systematic analysis for heavier nuclei along with the development of precise empirical interactions fitted to describe recent experimental data should help to elucidate whether such a picture also holds in model spaces involving high-j orbitals.

ACKNOWLEDGMENTS

K.H. thanks the FWO-Vlaanderen for financial support. This research was performed in the framework of the BriX network (P6/23) funded by the "IUAP Programme—Belgian State-BSP." N.S., K.S., and F.N. acknowledge the financial support of the CFT (CNRS/IN2P3), France.

[1] E. Caurier *et al.*, Rev. Mod. Phys. **77**, 427 (2005).
[2] O. Sorlin and M.-G. Porquet, Prog. Part. Nucl. Phys. **61**, 602 (2008).
[3] R. Kruecken, Contemp. Phys. **52**, 101 (2011).
[4] G. Neyens, Rep. Prog. Phys. **66**, 633 (2003).
[5] A. Gade and T. Glasmacher, Prog. Part. Nucl. Phys. **60**, 161 (2008).
[6] A. Goergen, J. Phys. G **37**, 103101 (2010).

[7] T. Baumann, A. Spyrou, and M. Thoenessen, Rep. Prog. Phys. **75**, 036301 (2012).
[8] B. A. Brown, Prog. Part. Nucl. Phys. **47**, 517 (2001).
[9] T. Otsuka *et al*., Prog. Part. Nucl. Phys. **47**, 319 (2001).
[10] M. Bender, P.-H. Heenen, and P.-G. Reinhard, Rev. Mod. Phys. **75**, 121 (2003).
[11] T. Niksic, D. Vretenar, and P. Ring, Prog. Part. Nucl. Phys. **66**, 519 (2011).
[12] J.-P. Delaroche *et al*., Phys. Rev. C **81**, 014303 (2010).
[13] S. M. Lenzi, F. Nowacki, A. Poves, and K. Sieja, Phys. Rev. C **82**, 054301 (2010).
[14] K. Heyde and J. L. Wood, Rev. Mod. Phys. **83**, 1467 (2011).
[15] T. Otsuka, R. Fujimoto, Y. Utsuno, B. A. Brown, M. Honma, and T. Mizusaki, Phys. Rev. Lett. **87**, 082502 (2001).
[16] T. Otsuka, T. Suzuki, R. Fujimoto, H. Grawe, and Y. Akaishi, Phys. Rev. Lett. **95**, 232502 (2005).
[17] T. Otsuka and D. Abe, Prog. Part. Nucl. Phys. **59**, 425 (2007).
[18] A. Umeya and K. Muto, Phys. Rev. C **69**, 024306 (2004).
[19] A. Umeya and K. Muto, Phys. Rev. C **74**, 034330 (2006).
[20] T. Otsuka, T. Suzuki, M. Honma, Y. Utsuno, N. Tsunoda, K. Tsukiyama, and M. Hjorth-Jensen, Phys. Rev. Lett. **104**, 012501 (2010).
[21] N. A. Smirnova *et al*., Phys. Lett. B **686**, 109 (2010).
[22] M. Hjorth-Jensen, T. T. S. Kuo, and E. Osnes, Phys. Rep. **261**, 125 (1995).
[23] S. K. Bogner, T. T. S. Kuo, and A. Schwenk, Phys. Rep. **386**, 1 (2003).
[24] A. Schwenk and A. P. Zuker, Phys. Rev. C **74**, 061302 (2006).
[25] A. P. Zuker, Phys. Rev. Lett. **90**, 042502 (2003).
[26] T. Otsuka, T. Suzuki, J. D. Holt, A. Schwenk, and Y. Akaishi, Phys. Rev. Lett. **105**, 032501 (2010).
[27] J. D. Holt, T. Otsuka, A. Schwenk, and T. Suzuki, J. Phys. G **39**, 085111 (2012).
[28] R. K. Bansal and J. B. French, Phys. Lett. **11**, 145 (1964).
[29] A. Poves and A. P. Zuker, Phys. Rep. **70**, 235 (1981).
[30] A. P. Zuker and M. Dufour, arXiv:nucl-th/9505012.
[31] M. Baranger, Nucl. Phys. A **149**, 225 (1970).
[32] T. Duguet and G. Hagen, Phys. Rev. C **85**, 034330 (2012).
[33] M. Dufour and A. P. Zuker, Phys. Rev. C **54**, 1641 (1996).
[34] P. Federman and S. Pittel, Phys. Rev. C **20**, 820 (1979).
[35] T. Lesinski, M. Bender, K. Bennaceur, T. Duguet, and J. Meyer, Phys. Rev. C **76**, 014312 (2007).
[36] M. Bender, K. Bennaceur, T. Duguet, P.H. Heenen, T. Lesinski, and J. Meyer, Phys. Rev. C **80**, 064302 (2009).
[37] V. Hellemans, P.-H. Heenen, and M. Bender, Phys. Rev. C **85**, 014326 (2012).
[38] P. Navratil, V. G. Gueorguiev, J. P. Vary, W. E. Ormand, and A. Nogga, Phys. Rev. Lett. **99**, 042501 (2007).
[39] J. P. Elliott *et al*., Nucl. Phys. A **121**, 241 (1968).
[40] M. W. Kirson, Phys. Lett. B **47**, 110 (1973).
[41] K. Klingenbeck *et al*., Phys. Rev. C **15**, 1483 (1977).
[42] K. Yoro, Nucl. Phys. A **333**, 67 (1980).
[43] B. A. Brown, W. A. Richter, and B. H. Wildenthal, J. Phys. G **11**, 1191 (1985).
[44] E. Osnes and D. Strottman, Phys. Rev. C **45**, 662 (1992).
[45] F. Nowacki and A. Poves, Phys. Rev. C **79**, 014310 (2009).
[46] B. A. Brown and B. H. Wildenthal, Annu. Rev. Nucl. Part. Sci. **38**, 29 (1988).
[47] J. Retamosa, E. Caurier, F. Nowacki, and A. Poves, Phys. Rev. C **55**, 1266 (1997).
[48] M. Honma, T. Otsuka, B. A. Brown, and T. Mizusaki, Phys. Rev. C **65**, 061301(R) (2002).
[49] B. A. Brown and W. A. Richter, Phys. Rev. C **74**, 034315 (2006).
[50] T. T. S. Kuo and G. E. Brown, Nucl. Phys. **114**, 241 (1968).
[51] R. Machleidt, Phys. Rev. C **63**, 024001 (2001).
[52] A. Poves *et al*., Nucl. Phys. A **694**, 157 (2001).
[53] B. S. Nara Singh *et al*., Phys. Rev. Lett. **107**, 172502 (2011).
[54] P. Boutachkov *et al*., Phys. Rev. C **84**, 044311 (2011).
[55] C. Hinke *et al*., Nature (London) **486**, 341 (2012).
[56] N. Tsunoda, T. Otsuka, K. Tsukiyama, and M. Hjorth-Jensen, Phys. Rev. C **84**, 044322 (2011).